Hindawi Publishing Corporation
Journal of Applied Mathematics
Volume 2012, Article ID 268371, 12 pages
doi:10.1155/2012/268371

Research Article

A Numerical Study on Flow around Nonuniform Porous Fences

Long-Ming Huang,[1] H. C. Chan,[1] and Jung-Tai Lee[2]

[1] *Department of Soil and Water Conservation, National Chung Hsing University, Taichung 40227, Taiwan*
[2] *Sinotech Engineering Consultants, Ltd., 12th Floor, 171 Nanking E. Road. Section 5, Taipei 10570, Taiwan*

Correspondence should be addressed to Jung-Tai Lee, lee2406@mail.sinotech.com.tw

Received 15 February 2012; Accepted 27 May 2012

Academic Editor: Shuyu Sun

The effects of a porous fence with a nonuniform porosity on flow fields are investigated numerically. First, an experiment with a non-uniform porous fence located in a wind tunnel is performed to obtain a reference data set. Then, a numerical model that utilizes the finite volume scheme with a weakly compressible-flow method to solve the continuity and momentum equations is developed. The numerical simulation is compared to experimental measurements for validation purposes. As a result, the numerical predictions show good agreements with the experimental data. Finally, the numerical investigations of the flow fields around porous fences with various combinations of upper and lower fence porosity are also presented. When the upper porosity is greater than the lower porosity, the Protection Index $PI_{0.1}$, $PI_{0.3}$ and $PI_{0.5}$, representing the adverse sheltering effect, decreases compared to that of the uniform porous fence. When the upper porosity is less than the lower porosity, the $PI_{0.5}$ increases and the variations of the $PI_{0.1}$ and $PI_{0.3}$, depend on the upper porosity, compared to that of the uniform porous fence. The results show that the porous fence with the upper fence porosity $\varepsilon_U = 0\%$ and the lower fence porosity $\varepsilon_L = 30\%$ gives the best sheltering effect among the porous fences in this study.

1. Introduction

Various kinds of fences have been used as windbreaks to reduce the wind erosion effectively. A fence blocks the oncoming flow and reduces the mean velocity of the flow behind the fence. Flows around a fence are of complex characteristics. Flow separation from fences results in strong shear layers, along which turbulence intensities are large. *The high turbulence level and the shear layer of the recirculation flow in the near wake region.* Variations of fence porosity are not only to modify the flow velocity but also to control the turbulence structure around the fence. In order to evaluate the sheltering effect properly and efficiently, a deeper understanding of the underlying dynamics of the turbulent structures is required.

The characteristics of turbulent flows around porous fences have been reported in several studies [1–4]. Raine and Stevenson [3] measured the mean and turbulent

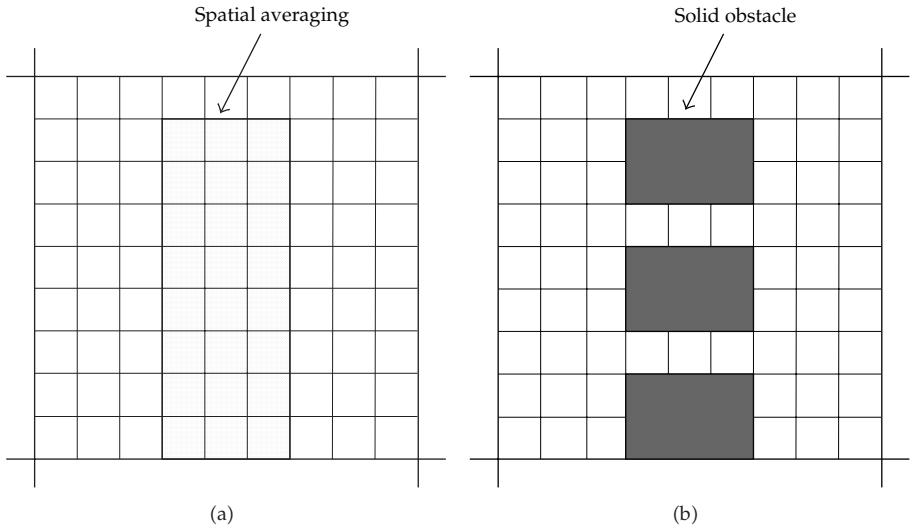

Figure 1: How to handle the porous fence. (a) Reproduced as a drag law. (b) Directly reproduced configuration.

characteristics of wake flow behind various porous fences. They classified the wake flow into two regions: the bleed flow dominant region and the displacement flow dominant region. Additionally, porous fences with low to medium porosities were more effective in reducing the mean velocity more than the solid one. Perera [1] experimentally investigated the flow around various porous fences immersed in a simulated atmospheric boundary layer. The porosity of the fence was the most significant parameter on the recirculation characteristics behind the fence, compared to other factors required for the fence design. Castro [2] and Perera [1] showed that the recirculation flow behind the porous fence disappeared when the fence porosity was more than $\varepsilon = 30\%$. Yaragal et al. [4] measured the flow fields downstream of both solid and porous fences. The fluctuating pressure of the porous fence with $\varepsilon = 60\%$ was by about 50% less than that of the solid fence. By measuring the mean velocity and turbulence intensity profiles, Lee et al. [5] found that the porous wind fence with porosity $\varepsilon = 30\%$ was most effective in abating windblown sand particles.

The above experimental results demonstrated that the characteristics of turbulent flow downstream of the porous fence significantly depended on the porosities. Hence, the numerical model will meet some considerable both in modeling the fluid dynamics of the recirculation flow and the porous effects. Usually, practical engineers used a drag law to represent the porous effects due to low computational cost [6–9]. With such a drag law, only the spatial averaged flow structures around porous fences are provided (Figure 1(a)). *The application of drag law needs to correctly acquire drag coefficients in the momentum equation.* However, very little drag data of porous fences are available. Application of the numerical model with a drag law to predicate the local flows around porous fences is rather difficult. In other previous studies, the flows around porous fences were solved at a local level [10]. The computational grids lie well inside the holes of porous fences and hence flow characteristics are calculated both inside and around the holes (Figure 1(b)). The primary application of these models is to model the interactions between the flow through the holes and the recirculation flow.

The above literature demonstrates the detailed investigation of the flow structures around porous fences, and the role played by the porosity has been emphasized. However,

data for the cases of a porous fence with a nonuniform porosity are limited. An elevated fence constructed in a road becomes nonuniform when support structures create a gap between the bottom of the fence and the ground. Also, the solid fences act as nonuniform porous fences when it receives a strong wind during its construction. Cho [11] pointed out that a fence with a bottom gap was cost effective in reducing the surface shear stress behind a porous fence. Park and Lee [12] experimentally investigated the turbulent flow behind the porous fences with nonuniform porosities. In their study, they focused on the effects of fence gap on the surface pressure characteristics behind the fences rather than exhibiting the flow structures and their interactions with the porous fences.

The main objective of this study is to numerically investigate the effects of porous fences with nonuniform porosities on flow structures, by varying the porosity in the upper and lower halves of a fence. We recognized in literature survey that no experimental data was available for examining the performance of a model predicting flow through a nonuniform porous fence. Therefore, experimental results with a nonuniform porous fence are presented to provide a reference data set for validating the numerical model. The validated numerical model is used to study the sheltering effect of a nonuniform porous fence. The Protection Index described by Van et al. [13], evaluated from the area of the reduced mean streamwise velocity behind a fence, is introduced to examine the performance of a porous fence. The present findings are expected to provide proper guidance in the design of porous fences with nonuniform porosities.

2. Experimental Apparatus and Methods

The experiments were conducted in an open-suction-type wind tunnel with a test section of 0.6 W × 0.6 H × 8.0 L (m^3). Spires and roughness elements were installed in front of the test section to create a thermally neutral atmospheric boundary layer. A porous fence with a nonuniform porosity was tested. The porosity of the lower half of the porous fence (ε_L) was 30%, while the upper half was solid and upper porosity (ε_U) was 0%. The porous fence had a height (H) of 6.0 cm and a flat end at the fence top. The porous fence extended the full width of the wind tunnel test section. Since the aspect ratio (height/width) of the porous fence is small (1/10), the model fence used in this study can be assumed to be two-dimensional (2D) one. The porous fence was installed at a position 6.0 m downstream of the inlet of the test section. A schematic diagram of the porous fence model and coordinate system used in this study is shown in Figure 2. The uniform inlet velocity U_0 was 10.60 m/sec and the Reynolds number Re_H based on the fence height H was about 4.1×10^4. A hot-wire anemometer (TSI IFA-300) with a probe (TSI 1241-T1.5) were used to measure the velocity profiles. A computer-controlled translation system was used to precisely locate and move the probe. The measurements were made at 36 points in the vertical, with distance from the bottom wall ranging from $0.05H$ to $7.5H$. The measurements at each location were instantaneous at a sampling frequency of 2 kHz for 20,000 data. These data were used to compute the statistical properties and would be compared with the corresponding numerical simulation.

3. Numerical Simulation

The flow characteristics depicted in Figure 1 can be carried out under a simplified condition. The porous fence extended the full width of the wind tunnel test section. It involves the 2-D turbulent flows around a porous fence. The governing equations are the continuity and

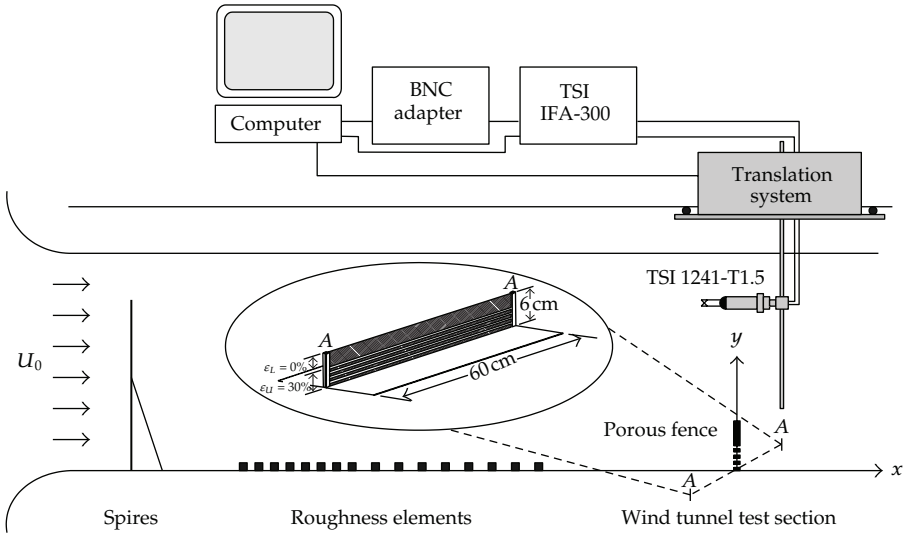

Figure 2: Schematic diagram of the porous fence and coordinate system.

momentum equations. The LES form of the dynamic subgrid-scale model by Germano et al. [14] is employed to take the turbulent effects into account. The numerical method used for the solution of the governing equations is developed on the basis of the finite volume scheme with a weakly compressible-flow method [15] in a Cartesian coordinate system. The governing equations of continuity and momentum are as follows:

$$\begin{aligned} \frac{\partial p}{\partial t} + k\nabla \cdot V &= 0 \\ \frac{\partial V}{\partial t} + V \cdot \nabla V &= -\nabla \frac{p}{\rho} + \nabla \cdot [(\nu + \nu_t)\nabla V], \end{aligned} \tag{3.1}$$

where p is the pressure; V denotes velocity components on each axis on the Cartesian coordinates; t is the time; k is the bulk modulus of elasticity of air; ν is the kinematic viscosity; ν_t is the turbulent eddy viscosity. The turbulent eddy viscosity is expressed as

$$\nu_t = (C_S \Delta)^2 \sqrt{2 S_{ij} S_{ij}} \quad \text{where } S_{ij} = \frac{1}{2}\left(\frac{\partial u_i}{\partial x_j} + \frac{\partial u_j}{\partial x_i}\right), \tag{3.2}$$

where C_S is the Smagorinsky coefficient; Δ denotes the characteristic length of the computational grid and the strain tensor S_{ij}. Based on the dynamic subgrid-scale model [14], two filters (grid and test filters) are used in the model calculations. The C_S, at the next time step, is determined through the comparison between the turbulent shear stresses resulting from different filters in a certain time step. The computational domain used in terms of the fence height H is $40H$ long and $10H$ high. The geometric characteristics used in the equations are the same ones used in the experiments. Figure 3 depicts an example of the grid system used in this study. Mesh distributions are all geometric progressions away from the regions of steep gradients, such as those close to the walls and around the holes of the fences. The

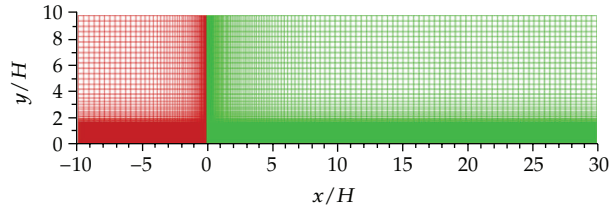

Figure 3: Grid system used in this study (green grids showing downstream of the fence; red grids showing upstream of the fence).

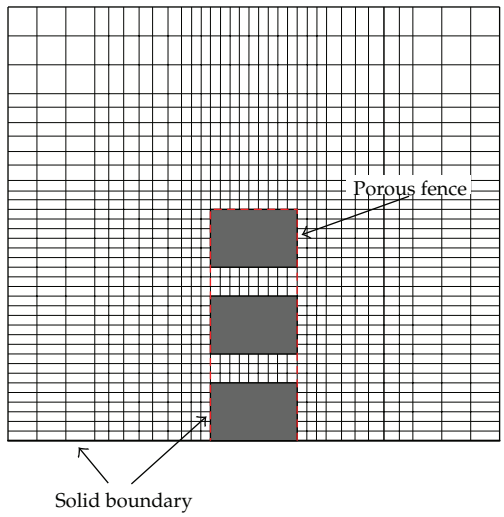

Figure 4: Computational grid local to the porous fence.

grid structure local to the porous region is shown in Figure 4. In this study, the numerical simulation particularly investigates the flow near a porous fence, which is difficult to be represented by treating the porous fence as a uniform area with a drag law. In order to reflect the physical nature of the boundaries, *the following boundary conditions are used in this study: a power-law velocity profile at the entrance; a reference pressure at the exit; a no-slip condition at the wall and the surface of the porous fence.*

4. Model Testing and Validation

Figure 5 shows the measured mean velocity profiles around the porous fence. The approaching flow is divided into two parts just in front of the fence. The deflected flow moves upward and passes above the fence top. In addition, the bleed flow passes through the holes of the lower half of the porous fence. A recirculation region with negative velocities exists behind the porous fence. Velocity profiles behind the porous fence show large velocity gradients existing at two vertical locations, one just above the structures and the other near the location of $y/H = 0.5$. The higher part indicates the separation from the top edge of the fence. The lower part attributes to the interaction between the bleed flow and the wall boundary layer. Meanwhile, the numerical model in this study was employed to simulate

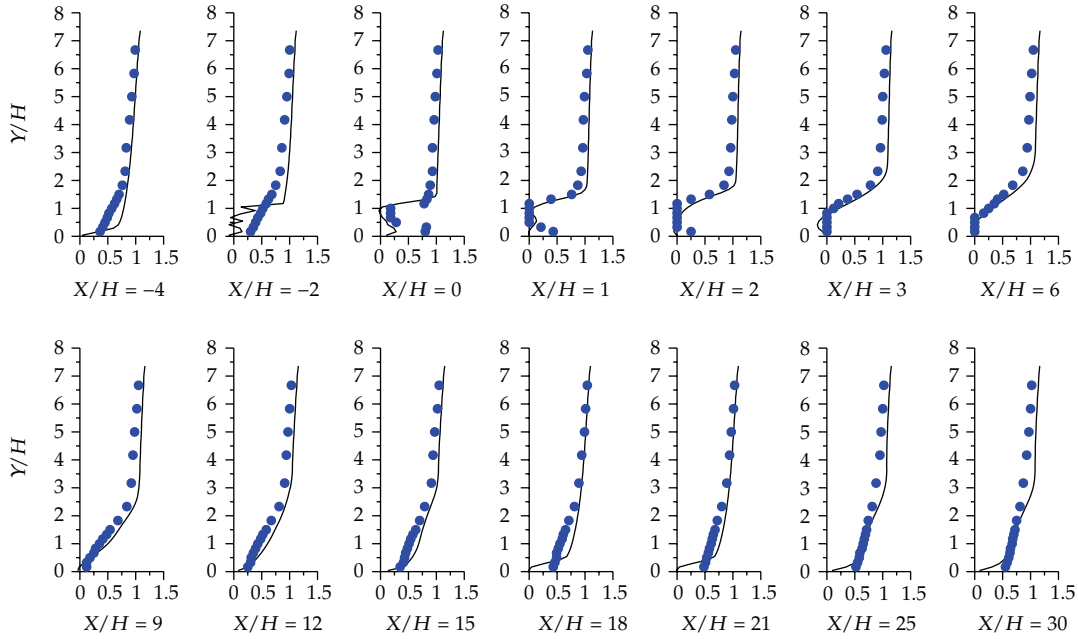

Figure 5: Comparison between calculated results and measured data of mean streamwise velocity profiles around the nonuniform porous fence (ε_U = 0% and ε_L = 30%): (full line) numerical simulation, (●) experiment.

the flow fields around nonuniform porous fences. The first run was performed under the experimental condition. *The numerical results were tested for grid independence by comparing the velocities obtained for* 301 × 46 *and* 351 × 51 *grid cells.* With these two grids, the results are quite close while the streamwise velocities near the porous fence reveal an averaged discrepancy of 1.2%. Therefore, all the following computations are carried out using a grid size of 351 × 51, and are expected to be grid independent. Figure 4 also shows the detailed comparison between the measured data and the corresponding computed results. Behind the porous fence, the bleed flow passing through the porous fence pushes the recirculation flow resulting in positive velocities near the wall, and the reversed flow phenomena disappear in the region $6 < x/H < 9$. This mixing interaction between the bleed flow and the recirculation flow is well-predicted using the present model. *The model gives slightly higher values than the measured data in the recirculation region. However, the general trends of velocity profiles and the locations of the peak value are well reproduced. The velocity distributions are in good agreement and measures can be evaluated for the main recirculation zone behind the fence. As shown in Figure 2, therefore, the porous fence was arranged in the wind tunnel with two vertical blocks from side walls. The LES is considered to be sufficiently validated to carry out the numerical simulations of turbulent flow passing through a porous fence.*

5. Results and Discussion

The numerical model in this study was validated by comparing the computed results with the experimental data. Future applications of the numerical model were to be the numerical analysis of the manipulated flow cases. The computational conditions, including the boundary conditions and model parameters, of the experiment in the previous section

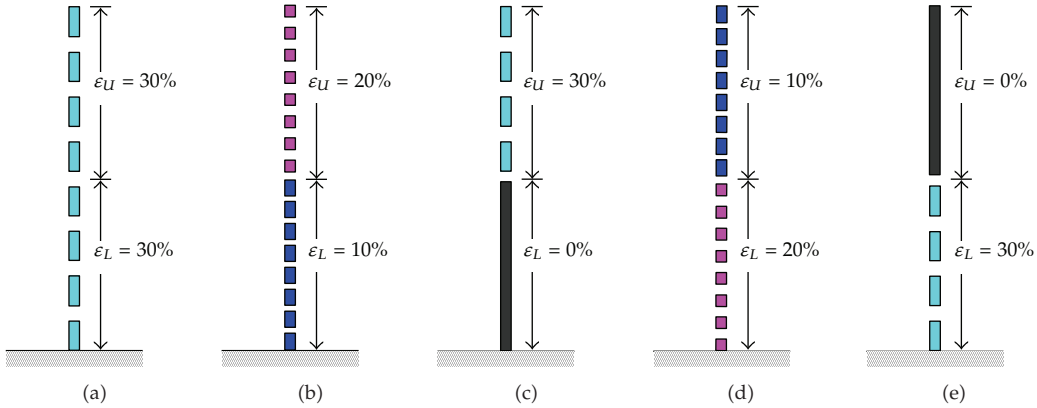

Figure 6: Porous fences: (a) $\varepsilon_U = 30\%$ and $\varepsilon_L = 30\%$; (b) $\varepsilon_U = 20\%$ and $\varepsilon_L = 10\%$; (c) $\varepsilon_U = 30\%$ and $\varepsilon_L = 0\%$; (d) $\varepsilon_U = 10\%$ and $\varepsilon_L = 20\%$; (e) $\varepsilon_U = 0\%$ and $\varepsilon_L = 30\%$.

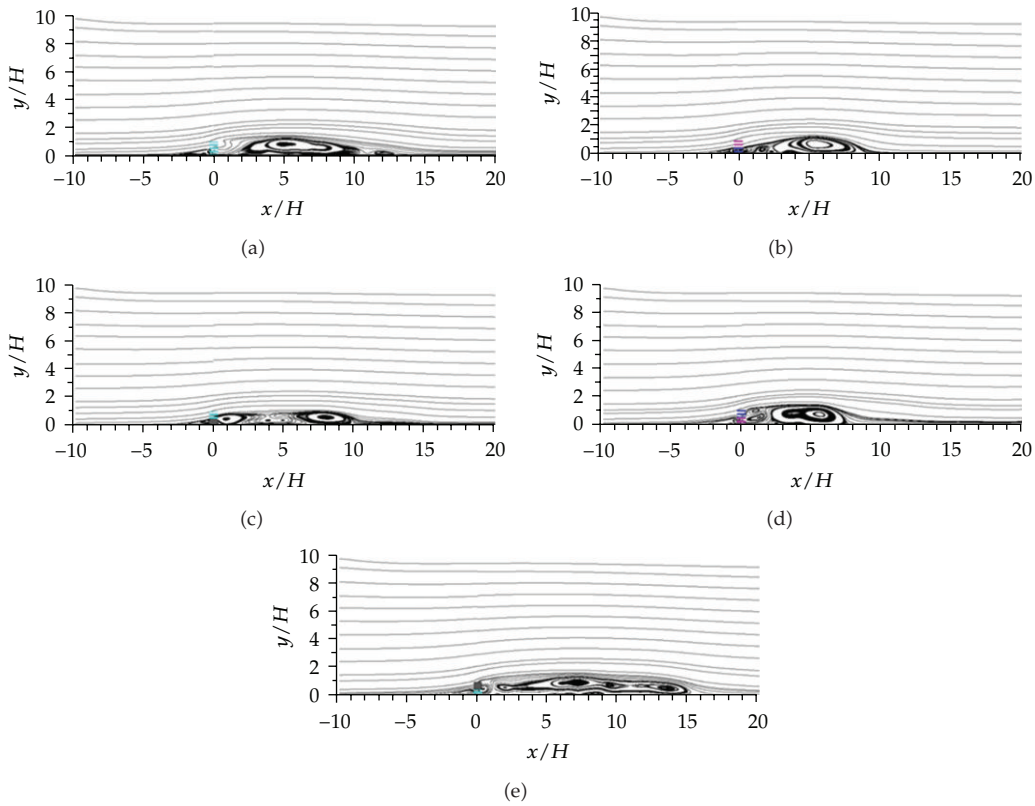

Figure 7: Comparison between calculated streamline patterns around various porous fences.

were used as the basis for the following numerical analysis. Various combinations of upper and lower fence porosity were numerically studied. Five porous fences and the combinations of upper and lower fence porosity used in this study are shown in Figure 6. *Figure 7 presents the mean streamline patterns around various porous fences.* For all the porous fences, the

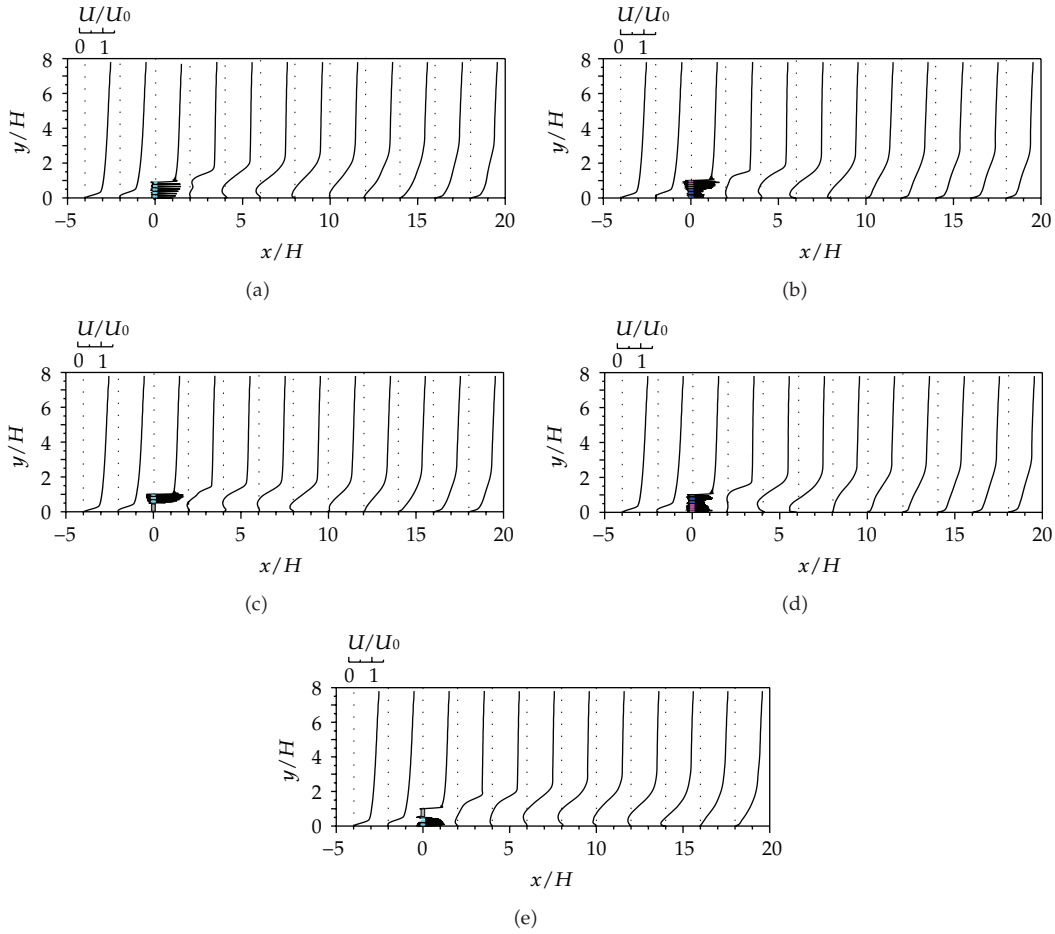

Figure 8: Variations of calculated mean streamwise velocity profiles around various porous fences.

streamlines are shifted and there is a recirculation flow region behind the fence. When the porous fence is nonuniform, the bleed flow has a velocity gradient in the vertical direction. This effect produces extra mixing interaction as the fluid passes through the fence holes. Therefore, the recirculation region is highly dependent of the combinations of fence porosity. This indicates that the manipulation of the bleed flow at either the upper or lower parts of the fence has a significant effect on the recirculation region but the mechanisms involved are different. Besides, the recirculation region behind the porous fence of case E is considerably larger than the other cases. Figures 8 and 9 show the variations of mean streamwise and vertical velocity profiles around porous fences. The results give the qualitative and quantitative observations of flow patterns passing through the porous fences. The bleed flow passing through porous holes facilitate jets toward the recirculation flow at high velocities. When the upper porosity is greater than the lower porosity, the bleed flow passing through the upper half of the fence increases. The strong bleed flow of the upper fence mixes with the shear layer separated from the top edge of the fence. Hence, the downward motion of the entrained shear flow is reduced. In cases B and C, the mean vertical velocities are smaller than that of the uniform porous fence. When the porosity of the upper half of the fence is

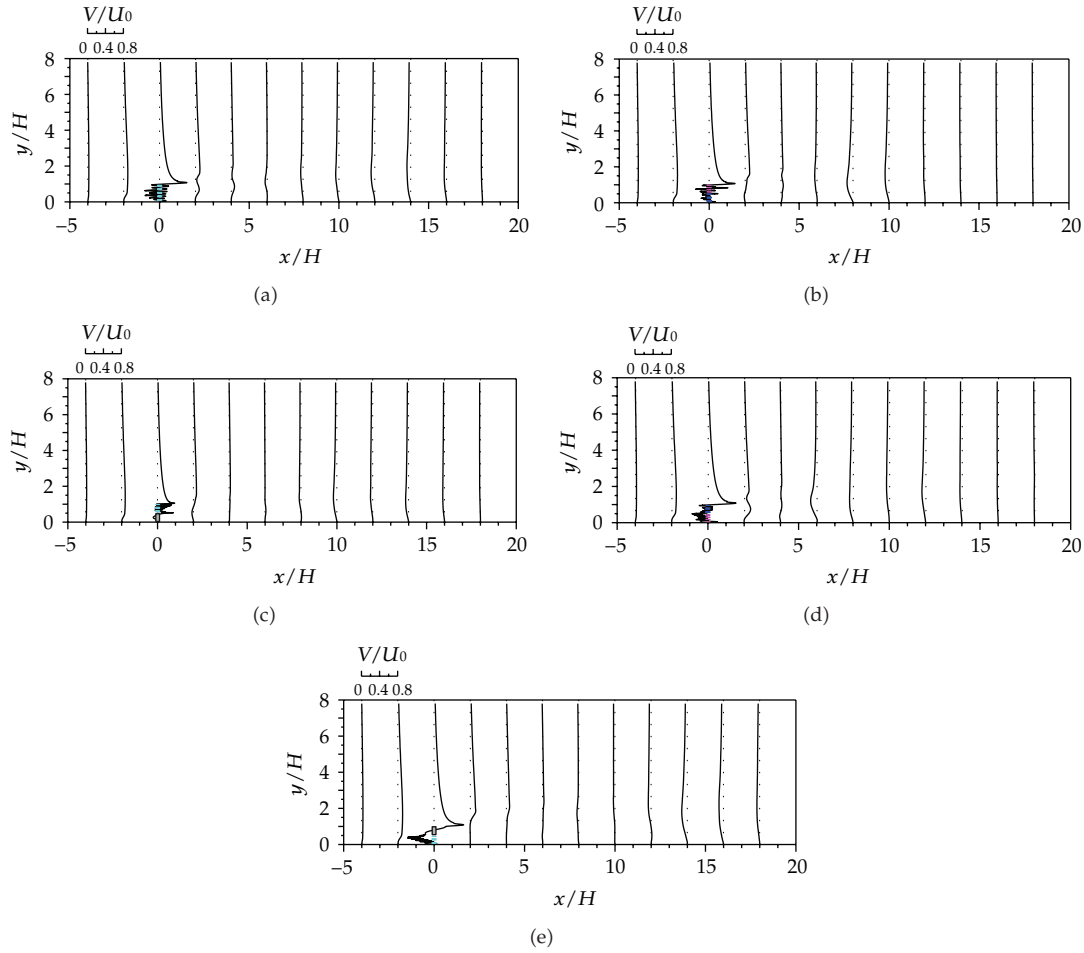

Figure 9: Variations of calculated mean vertical velocity profiles around various porous fences.

less than that of the lower half, the bleed flow passing through the lower fence becomes strong and gradually pushes up the recirculation flow. In cases D and E, the recirculation flow displays high vertical velocities in the region of $y/H < 0.5$. Contour plots of the mean streamwise velocity for the different fences are shown in Figure 10. For all porous fences, the approaching flow decelerates behind the fence. The optimal design of porous fences is determined by engineer's own purpose. For the main purpose of mean velocity reduction, Van et al. [13] had proposed a shelter parameter to quantify the sheltering effect of the fence. This index was evaluated from the areas under the $U/U_0 = 0.5$ contour line of the reduced mean streamwise velocity behind the fence. However, this index reflected only the streamwise mean velocity at one certain value. Although the areas under the other velocity level are relatively small compared to the areas under the $U/U_0 = 0.5$ contour line, it must be considered in addition to obtain an accurate shelter parameter. Therefore, this study takes into account three streamwise velocity levels. The contour lines are the best fit curves with a second-order polynomial. The corresponding areas under $U/U_0 = 0.1, 0.3$ and 0.5 behind the fences are represented by $PI_{0.1}$, $PI_{0.3}$, and $PI_{0.5}$, respectively, and summarized in Table 1.

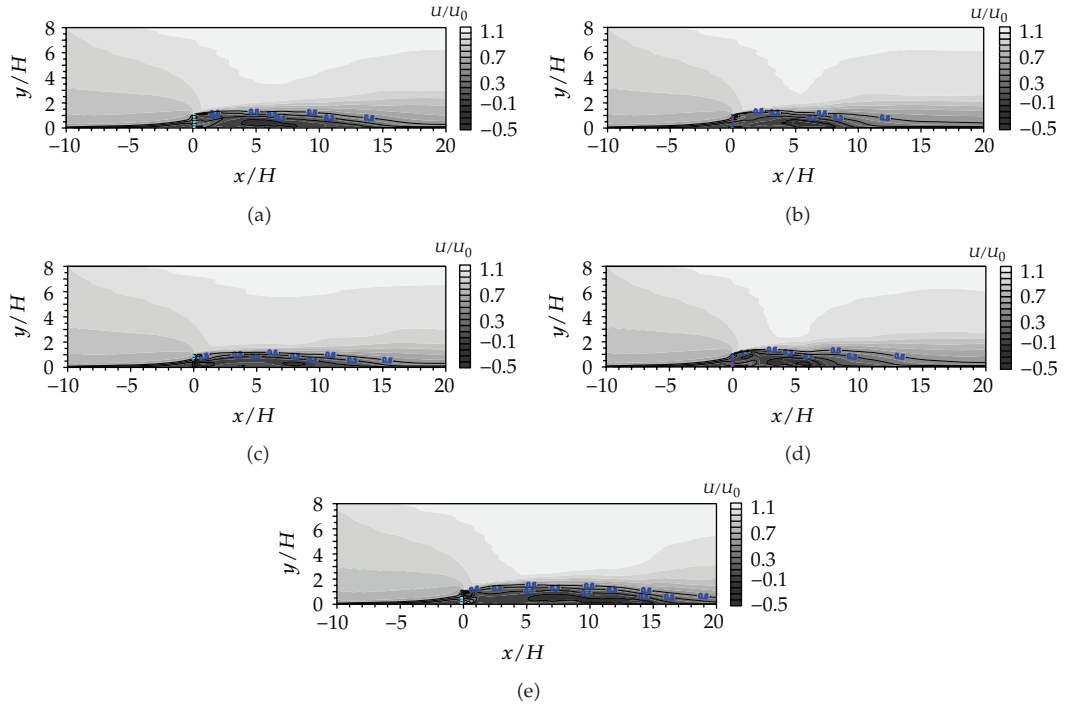

Figure 10: Contour plots of the calculated mean streamwise velocity for various porous fences.

Table 1: Areas under contours $U/U_0 = 0.1, 0.3$ and 0.5 behind the fences.

Protection Index (H^2)	Case				
	A	B	C	D	E
$PI_{0.1}$	9.44	7.44	8.56	7.78	14.49
$PI_{0.3}$	16.67	13.05	13.63	14.26	21.33
$PI_{0.5}$	22.97	21.92	20.96	24.06	28.37

The effects of nonuniform porosity are clearly shown in terms of the values of $PI_{0.1}$, $PI_{0.3}$, and $PI_{0.5}$. In the cases of the upper porosity being greater than the lower porosity, the values of $PI_{0.1}$, $PI_{0.3}$, and $PI_{0.5}$ are slightly smaller than that of the uniform fence (case A). This may be attributed to the downward shear flow affected by the bleed flow which reduces the length of the recirculation flow. The velocity contours are sensitive when the upper porosity is less than the lower porosity. In case D, $PI_{0.1}$ and $PI_{0.3}$ decrease but $PI_{0.5}$ increases, comparison with the respective ones of the uniform fence. In case E, however, all of the areas under the three velocity contours significantly increase. These clearly reveal that the manipulation of the bleed flow at the lower locations of the porous fence has a significant effect on the sheltering effect. The values of $PI_{0.5}$ increase by about 5% and 24% for cases D and E, respectively, compared to that of the uniform fence. case E has the highest value of $PI_{0.5}$ among the porous fences in this study.

6. Conclusion

Flows around nonuniform porous fences are numerically investigated. The numerical model developed in this work is based on the finite volume scheme with a weakly-compressible-flow method. Additionally, the experimental data of a nonuniform porous fence are presented mainly for the validation of the numerical model. As a result, the numerical model is shown to be useful and appropriate for predicting the flows around a nonuniform porous fence. The computation results are consistent with the experimental data. The effect of nonuniform porous fence on flow fields are simulated by varying the combinations of upper and lower fence porosity. The bleed flow passing through a nonuniform porous fence has a velocity gradient in the vertical direction. This manipulation of the bleed flow of the porous fence has a significant effect on the sheltering effect evaluated by the Protection Index. In the porous fences with the upper porosity being greater than the lower porosity, the Protection Index decreases compared to that of the uniform porous fence. Additionally, the porous fences with the upper porosity being less than the lower porosity effectively enhance the sheltering effect. The porous fence with the porosity of the upper half of fence is 0% and the lower half of fence is 30% demonstrates best performance in sheltering effect among the porous fences in this study.

Acknowledgments

The authors gratefully acknowledge Ching-Hua Yang, former master student of the National Chung Hsing University (Taiwan), who carried out the wind tunnel measurements. The J.-T. Lee would also like to thank the National Science Council (Taiwan) for providing financial support (NSC 100-2626-M-005-004-MY3) during preparing this paper.

References

[1] M. D. A. E. S. Perera, "Shelter behind two-dimensional solid and porous fences," *Journal of Wind Engineering and Industrial Aerodynamics*, vol. 8, no. 1-2, pp. 93–104, 1981.

[2] I. P. Castro, "Wake characteristics of two-dimensional perforated plates normal to an air-stream," *The Journal of Fluid Mechanics*, vol. 46, pp. 599–609, 1971.

[3] J. K. Raine and D. C. Stevenson, "Wind protection by model fences in a simulated atmospheric boundary layer," *Journal of Industrial Aerodynamics*, vol. 2, no. 2, pp. 159–180, 1977.

[4] S. C. Yaragal, H. S. Govinda Ram, and K. Keshava Murthy, "An experimental investigation of flow fields downstream of solid and porous fences," *Journal of Wind Engineering and Industrial Aerodynamics*, vol. 66, no. 2, pp. 127–140, 1997.

[5] S. J. Lee, K. C. Park, and C. W. Park, "Wind tunnel observations about the shelter effect of porous fences on the sand particle movements," *Atmospheric Environment*, vol. 36, no. 9, pp. 1453–1463, 2002.

[6] A. R. Packwood, "Flow through porous fences in thick boundary layers: comparisons between laboratory and numerical experiments," *Journal of Wind Engineering and Industrial Aerodynamics*, vol. 88, no. 1, pp. 75–90, 2000.

[7] S. J. Lee and H. C. Lim, "A numerical study on flow around a triangular prism located behind a porous fence," *Fluid Dynamics Research*, vol. 28, no. 3, pp. 209–221, 2001.

[8] R. H. Shaw and U. Schumann, "Large-eddy simulation of turbulent flow above and within a forest," *Boundary-Layer Meteorology*, vol. 61, no. 1-2, pp. 47–64, 1992.

[9] T. Maruyama, "Large eddy simulation of turbulent flow around a windbreak," *Journal of Wind Engineering and Industrial Aerodynamics*, vol. 96, no. 10-11, pp. 1998–2006, 2008.

[10] S. Alhajraf, "Computational fluid dynamic modeling of drifting particles at porous fences," *Environmental Modelling and Software*, vol. 19, no. 2, pp. 163–170, 2004.

[11] H. M. Cho, *Wind-tunnel and numerical simulation of flow over porous fences and particle saltation in atmospheric boundary layer [Ph.D. thesis]*, Department of Mechanical and Aeronautical Engineering, University of California at Davis, Davis, Calif, USA, 1996.

[12] C. W. Park and S. J. Lee, "The effects of a bottom gap and non-uniform porosity in a wind fence on the surface pressure of a triangular prism located behind the fence," *Journal of Wind Engineering and Industrial Aerodynamics*, vol. 89, no. 13, pp. 1137–1154, 2001.

[13] E. J. Van, R. Karschon, L. A. Razumova, and G. W. Roberts, "Windbreaks and Shelterbelts," W. M. O. Technical note no. 59, Geneva, Switzerland, 1964.

[14] M. Germano, U. Piomelli, P. Moin, and W. H. Cabot, "A dynamic subgrid-scale eddy viscosity model," *Physics of Fluids A*, vol. 3, no. 7, pp. 1760–1765, 1991.

[15] C. C. S. Song and M. Yuan, "A weakly compressible flow model and rapid convergence methods," *Journal of Fluids Engineering*, vol. 110, pp. 441–455, 1988.